

Selective Visualization of Vortices in Hydrodynamic Flows

I. Ari Sadarjoen¹

Frits H. Post¹

Bing Ma²

David C. Banks³

Hans-Georg Pagendarm⁴

Abstract

Vortices are important features in many research and engineering fields. Visualization is an important step in gaining more understanding and control of vortices. Vortex detection criteria fall into two categories: point-based scalar quantities, calculated at single points, and curve-based geometric criteria, calculated for e.g. streamlines. The first category is easy to compute, but does not work in all cases. The second category is more intuitive and should work in all cases, but currently only works in 2D (or 3D projected) flows. We show applications of both approaches in hydrodynamic flows.

1 Introduction

Vortices are important features in flow research, and they are studied for theoretical and practical purposes. In fundamental flow research, the evolution of vortices is of great importance. In engineering designs, vortices can either be desirable or undesirable, and designs are optimized to prevent or to promote the occurrence of vortices. Visualization of vortices is therefore important for understanding the underlying physics, and also for simulating and modifying designs. Previous applications of vortex detection and visualization have been described in oceanography [12], aerodynamics [5], and turbomachinery design [10].

Informally, a vortex is defined as a swirling flow pattern which will often behave as a coherent structure in time-dependent flows. A formal definition of a vortex cannot be easily given. Although in fluid dynamics research, several criteria have been developed for their detection, the essential characteristics are hard to capture, and none of the existing criteria is entirely satisfactory.

The criteria can be roughly classified in two groups:

- point-based criteria, for which a local quantity is sampled or calculated at a given point in a flow field,
- curve-based criteria, using local geometric properties of streamlines.

In this case study, we will briefly characterize these types of criteria, and suggest a selective approach toward vortex detection and visualization for both types of criteria. Selection expressions are evaluated at grid nodes (as described in [11]), but can also be used with points on streamlines. We will show some results of applications in hydrodynamics, with these different types of detection criteria.

2 Vortex Detection Criteria

The first category of detection criteria is *point-based*, and consists of scalar quantities that can be determined at each point in a flow

field. They are based on assumptions about the characteristics of the flow patterns in an (infinitely) small zone around a point. Examples of this type are pressure, vorticity, and various quantities derived from the velocity gradient tensor $\nabla\mathbf{v}$. Brief surveys have been given by Banks and Singer [1] and Roth and Peikert [10]. All of these criteria are formal, and can be applied to points where the required quantities can be calculated. However, they sometimes fail to detect obvious vortices, or they find non-vortical structures. A reason for this may be that a vortex is essentially a macroscopic or regional phenomenon, and the point samples underlying the criteria do not always translate into regional characteristics.

Examples of point-based criteria that we have used are:

- low pressure
- high vorticity magnitude: $\omega = |\nabla \times \mathbf{v}|$
- high normalized helicity: $h_n = \frac{\mathbf{v} \cdot \omega}{|\mathbf{v}| |\omega|}$
- negative λ_2 , defined as the second largest eigenvalue of the tensor $S^2 + \Omega^2$, where $S = \frac{1}{2}(\nabla\mathbf{v} + (\nabla\mathbf{v})^T)$ is the symmetric part, and $\Omega = \frac{1}{2}(\nabla\mathbf{v} - (\nabla\mathbf{v})^T)$ the anti-symmetric part of the velocity gradient $\nabla\mathbf{v}$. Regions of negative λ_2 are considered vortical regions [4].
- positive Q , which is the second invariant of the velocity gradient tensor $\nabla\mathbf{v}$, defined as $Q = \frac{1}{2}(|\Omega|^2 - |S|^2)$, with the same Ω and S as above. Regions of positive Q are considered vortical regions [4].

The second category of criteria is *curve-based*, and tries to build upon the intuitive idea of a swirling pattern around a central set of points [8]. The criteria are based on geometric or kinematic flow characteristics, as represented by the shape of instantaneous streamlines. Robinson's definition is: "a vortex exists when instantaneous streamlines mapped onto a plane normal to the vortex core exhibit a roughly circular or spiral pattern, when viewed from a frame of reference moving with the center of the vortex core" [9]. When we look at Figure 3, the vortices are immediately obvious, but more formal criteria are needed. These can be derived from the differential geometric properties of streamlines.

Two curve-based criteria are curvature center density and winding-angle. The curvature center density (CCD) is based on [2]: at a number of points on a streamline, the center of curvature of its osculating circle is determined. If the streamline is (nearly) circular, the curvature centers will be concentrated in a region or even coincide, which indicates the presence of a vortex. See Figure 1a. If the streamline is not circular, the curvature centers will be scattered in space, which indicates the absence of a vortex. See Figure 1b. The local density of curvature centers can be accumulated into a grid, resulting in a discrete scalar field called the Curvature Center Density (CCD) field. High value of curvature centers in this field may then indicate a vortex.

The winding-angle (α_w) is based on a simplification of Portela's work [8]. Closed streamlines can be recognized by determining if the winding-angle of a streamline has reached 2π , and the end point lies near the initial point. The winding-angle of a (projected) streamline is the cumulative change of direction of the curve, or in other words, the sum of the signed angles between the line segments it consists of: $\alpha_w = \sum_i \alpha_i$, with $\alpha_i = \angle(\mathbf{p}_i, \mathbf{p}_{i+1})$, as illustrated in Figure 2. Obviously, $\alpha_w = 2\pi$ for a fully closed curve, but lower values may be used to find winding streamlines which do not make a full revolution.

¹Dept. of Computer Science, Delft University of Technology, Zuidplantsoen 4, 2628 BZ Delft. E-mail: sadarjoen@cs.tudelft.nl

²Lab. for Aero and Hydrodynamics, Delft University of Technology, and Tsinghua University, Beijing, P.R. China

³Dept. of Computer Science, Mississippi State University

⁴DLR: Deutsches Zentrum für Luft- und Raumfahrt (German Aerospace Center)

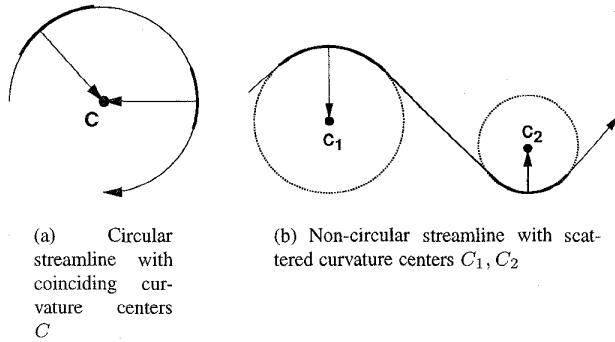


Figure 1: Streamlines with centers of curvature

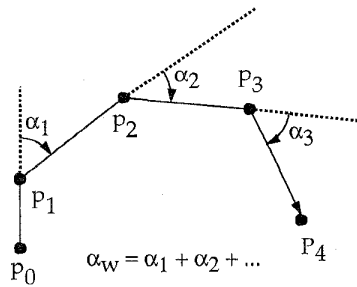


Figure 2: The winding-angle α_w of a piecewise linear curve is the sum of the angles α_i between adjacent line segments p_i, p_{i+1}

These criteria are intuitively appealing, but they have currently only been implemented in 2D. Therefore, we have used both point-based criteria and curve-based criteria.

For the point-based criteria and the CCD field, selection is made using the techniques developed in [11], which selects grid nodes that satisfy complex Boolean expressions involving scalar, vector, and tensor quantities defined at the nodes. The winding-angle criterion is combined with distance criteria to determine if a streamline end point lies near its initial point.

3 Applications and Results

We have applied techniques from both categories to a number of hydrodynamic data sets resulting from simulations of the Bay of Gdańsk, the Pacific Ocean, and a transitional pipe flow.

Bay of Gdańsk

The first application is a simulation performed at WL | Delft Hydraulics of the Bay of Gdańsk, a coastal area in Poland. The goal of the simulation was to investigate the flow patterns induced by wind, the inflow of the Vistula river, and turbulence [7]. The model is defined on a curvilinear grid of $43 \times 28 \times 20$ nodes, indexed by (i, j, k) . Each node contains a 3D velocity vector \mathbf{v} , an eddy-diffusivity scalar E , and its gradient ∇E . Figure 3 shows a top view of a 2D horizontal slice at the center of the grid, where $k=9$, with global streamlines released from all the grid nodes in this slice. A distinct number of large vortices are clearly visible to the human observer.

Unfortunately, point-based methods did not prove to be very successful in extracting these vortices. In a large number of experiments with point-based scalar quantities, such as the vorticity ω ,

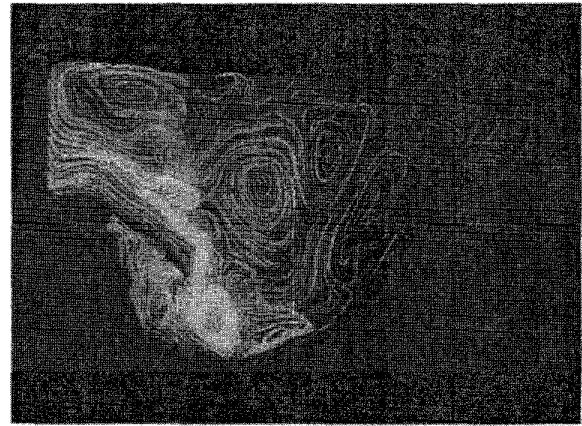


Figure 3: Bay of Gdańsk with global streamlines released in a horizontal slice where $k = 9$

helicity density h_n , and λ_2 , the best results were obtained with λ_2 . Then, starting from grid nodes where $\lambda_2 < -0.01$, selective streamlines were traced, which are shown in Figure 4. It can be seen that these streamlines based on λ_2 indicate some of the vortices, but by no means all of them; especially the weaker (slowly-rotating) vortices are missing. Also, some streamlines are selected which are not circular at all. This may be attributed to the limited scope of the point-based criteria; some streamlines may have a very negative value of λ_2 at one point, without being circular anywhere else.



Figure 4: Bay of Gdańsk with streamlines traced from grid nodes where $\lambda_2 < -0.01$

In this case, a curve-based method proved to be more effective in extracting the vortices. We applied the winding-angle criterion described in Section 2 to the above global streamlines. The criterion selected streamlines for which $\alpha_w > \frac{3}{2}\pi$. Figure 5 shows the selected streamlines in black and the other ones in gray. It can be seen that this selection technique successfully captures all the vortices, including the weak ones. Finding all vortices, including the weak ones, is essential for achieving the goal of analyzing the mixing of fresh and salt water, and the material deposition in the Bay near the mouth of the river.

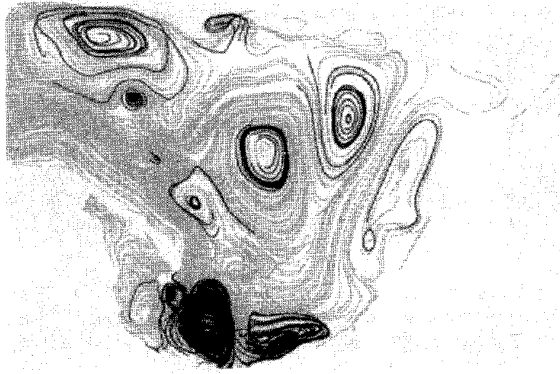


Figure 5: Bay of Gdańsk with selective streamlines using a winding-angle of $\alpha_w > \frac{3}{2}\pi$

Pacific Ocean

The next application is a numerical flow simulation of the Pacific Ocean, also used in [12]. The simulation employs the US Navy layered ocean model, a tool used by the Naval Oceanographic and Atmospheric Research Laboratory to assist in ocean prediction [3]. The data set used here concerns the surface layer of a subregion which models the western coast of North America, from 145°W to 110°W and from 15°N to 62°N . The grid used for the visualization is a 2D Cartesian grid consisting of 117x84 nodes, at each of which a 2D velocity vector is defined and a Boolean indicating whether the node is inside the flow domain, rather than on the land. Figure 8 (see Color Plate) shows the global flow pattern using streamlines released from every grid point and colored with velocity magnitude.

To detect vortices, we applied both curve-based methods. The first method calculated a curvature center density (CCD) field as described in the previous section. Then, thresholding was applied to select the regions where the curvature center density is relatively high: $CCD > 0.8 \cdot CCD_{max}$. Figure 8 renders this scalar field as a height field, showing only those selected peaks that satisfy the above criterion. It can be seen that this geometric method finds most of the strong and perfectly circular vortices, but not the weak or elongated ones.

The second method applied a winding-angle criterion of $\alpha_w > \frac{3}{2}\pi$ to the global streamlines of Figure 8. Figure 6 renders the selected streamlines in black and the other streamlines in gray. It can be seen that this method successfully captures almost all of the vortices, regardless of the rotation speed. Only very few non-vortices are captured.

Transitional Pipe Flow

The last application is a direct numerical simulation (DNS) of a transitional pipe flow, performed at the Laboratory for Aero- and Hydrodynamics of Delft University of Technology. Serving as a tool to explore the laminar-turbulent transition in pipe flows, the DNS tracks the spatial evolution of a local disturbance introduced from a wall area near the inflow. This disturbance consists of a Periodical Suctioning and Blowing (PSB) which causes streamwise vortex pairs to be generated. The evolution and breakdown of these vortices play an important role in the final transition to turbulent flow [6].

The simulation was performed on a 3D cylindrical grid consisting of $65 \times 17 \times 53$ nodes, indexed by (i, j, k) . For the visualization, we use only the part where $15 \leq i \leq 32$, with the disturbance being imposed at $i = 6$. The simulation calculated many quanti-

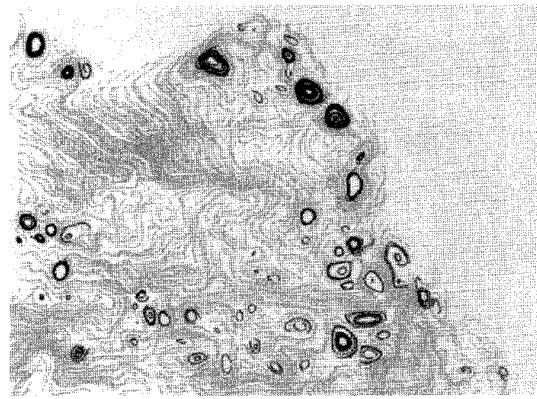


Figure 6: Pacific Ocean with selective streamlines using a winding-angle of $\alpha_w > \frac{3}{2}\pi$

ties at each node, but for the visualization we used: 3D velocity \mathbf{v} , vorticity magnitude ω , pressure P , λ_2 , and Q (see Section 2).

To visualize the results, we utilized both a point-based and a curve-based method. The point-based method comprises isosurfaces and selective streamlines. First, isosurfaces were drawn of a high value of Q (see Section 2). Then, we used the techniques from [11] to select grid nodes where Q has a higher value, and to trace streamlines through those nodes. By visually verifying if the streamlines are rotating, it can be checked if the isosurfaces are true vortices. Figure 9 (see Color Plate) shows a combined view with both semi-transparent isosurfaces of $Q = 0.05$, and selective streamlines through grid nodes where $Q \geq 0.05$. In contrast to the previous cases, this is an example where a point-based method for detecting vortices works well.

For the curve-based method, we applied the winding-angle criterion to streamlines released in the grid nodes of a transverse slice (where $i = 14$). As the winding-angle method is only suitable for 2D data, the streamlines were first projected along the cylinder axis onto the same slice. The winding-angle selected streamlines for which $\alpha_w > 1.3\pi$. Figure 7 shows the selected streamlines in black and the other ones in gray. As the vortices are not perfectly aligned to the projection direction, the results are not optimal, but still quite acceptable.

The visualization techniques here have proven a very helpful tool to reveal the physics behind these visual clues. The visualizations clearly show the streamwise vortex pairs. When viewing in the axial direction, it can be seen that the left and the right half of the pipe are symmetric, which indicates the correctness of the numerical simulation code. From side views, such as the one in Figure 9 (see Color Plate), it can be seen that the vortex pairs on the upper and lower walls alternate in the downstream direction, which reflects the imposed disturbance due to which the vortices are formed. Other visualizations showed that as these these vortex pairs travel downstream, they are deformed to long streamwise streaks. From the literature, these streaks are known to be highly unstable and to play an important role in the transition to turbulence.

4 Conclusions and Future Work

We have examined two types of vortex extraction criteria: point-based and curve-based criteria. The point-based criteria reveal vortical structures with varying degrees of success; sometimes they work very well, in other cases they fail. Stronger vortices with high angular velocity are usually found, but weaker vortices with low

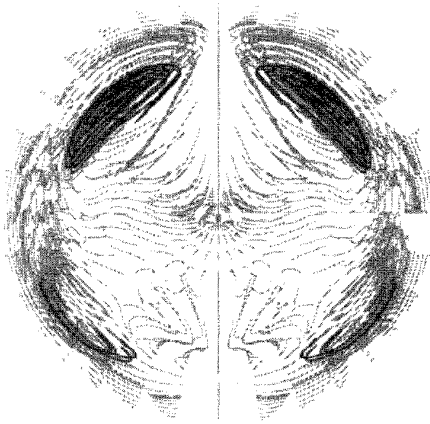


Figure 7: Pipe flow with selective streamlines using a winding-angle of $\alpha_w > 1.3\pi$

rotation speed, which are quite common in hydrodynamics, often remain undetected by most point-based techniques.

The curve-based criteria, especially the winding-angle method, look promising, even with the preliminary implementations available right now. The winding-angle method is largely insensitive to the rotation speed of a vortex, as only the geometric shape properties are considered.

References

- [1] D.C. Banks and B.A. Singer. Vortex tubes in turbulent flows: identification, representation, reconstruction. In *Proc. Visualization '94*, pages 132–139, 1994.
- [2] W.C. de Leeuw and F.H. Post. A statistical view on vector fields. In M. Göbel, H. Müller, and B. Urban, editors, *Visualization in Scientific Computing*, Eurographics, pages 53–62, Wien, 1995. Springer-Verlag.
- [3] H.E. Hurlburt, A.J. Wallcraft, Z. Sirkes, and E.J. Metzger. Modeling of the global and pacific oceans: On the path to eddy-resolving ocean prediction. *Oceanography*, 5:9–18, 1992.
- [4] J. Jeong and F. Hussain. On the identification of a vortex. *Journal of Fluid Mechanics*, 285:69–94, 1995.
- [5] D. Kenwright and R. Haimes. Vortex identification - applications in aerodynamics: A case study. In R. Yagel and H. Hagen, editors, *Proc. Visualization '97*. IEEE Computer Society Press, 1997.
- [6] B. Ma, C.W.H. van Doorne, Z. Zhang, and F.T.M. Nieuwstadt. On the evolution of wall-imposed periodic disturbance in pipe Poiseuille flow at $Re=3000$. *submitted to: Journal of Fluid Mechanics*, 1998.
- [7] A.E. Mynett, I.A. Sadarjoen, and A.J.S. Hin. Turbulent flow visualization in computational and experimental hydraulics. In G.M. Nielson and D. Silver, editors, *Proceedings Visualization '95*, pages 388–391, Los Alamitos, October 1995. IEEE Computer Society Press.
- [8] L.M. Portela. *On the Identification and Classification of Vortices*. PhD thesis, Stanford University, School of Mechanical Engineering, 1997.
- [9] S.K. Robinson. Coherent motions in the turbulent boundary layer. *Annual Review of Fluid Mechanics*, 23:601, 1991.
- [10] M. Roth and R. Peikert. Flow visualization for turbomachinery design. In R. Yagel and G.M. Nielson, editors, *Proc. Visualization '96*, pages 381–384. IEEE Computer Society Press, 1996.
- [11] T. van Walsum, F.H. Post, D. Silver, and F.J. Post. Feature extraction and iconic visualization. *IEEE Transactions on Visualization and Computer Graphics*, 2(2):111–119, 1996.
- [12] Z.F. Zhu and R.J. Moorhead. Extracting and visualizing ocean eddies in time-varying flow fields. In *Proceedings of the 7th International Conference on Flow Visualization*, Seattle, WA, Sept. 1995.

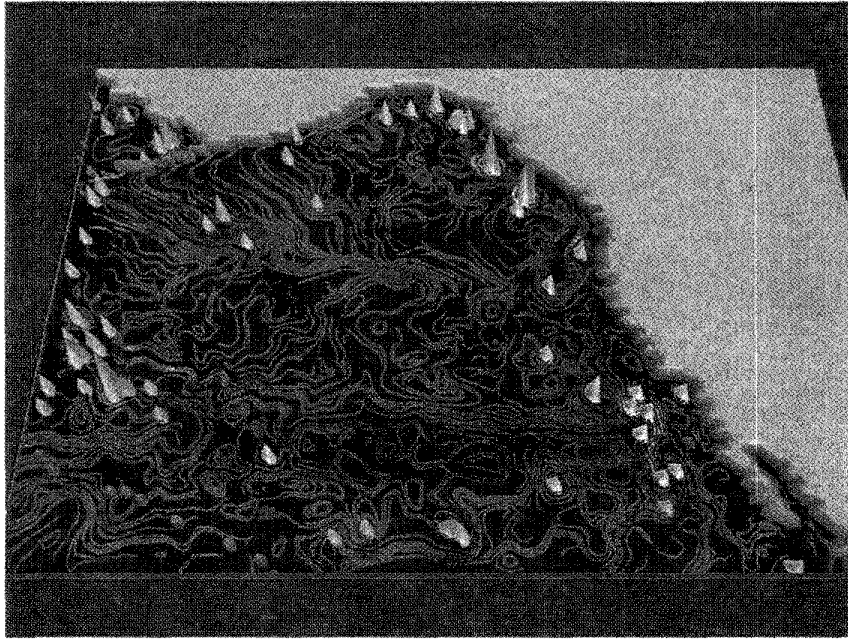


Figure 8: Pacific Ocean with global streamlines colored with velocity magnitude, and a white height field of curvature center density $CCD > 0.8 \cdot CCD_{max}$.

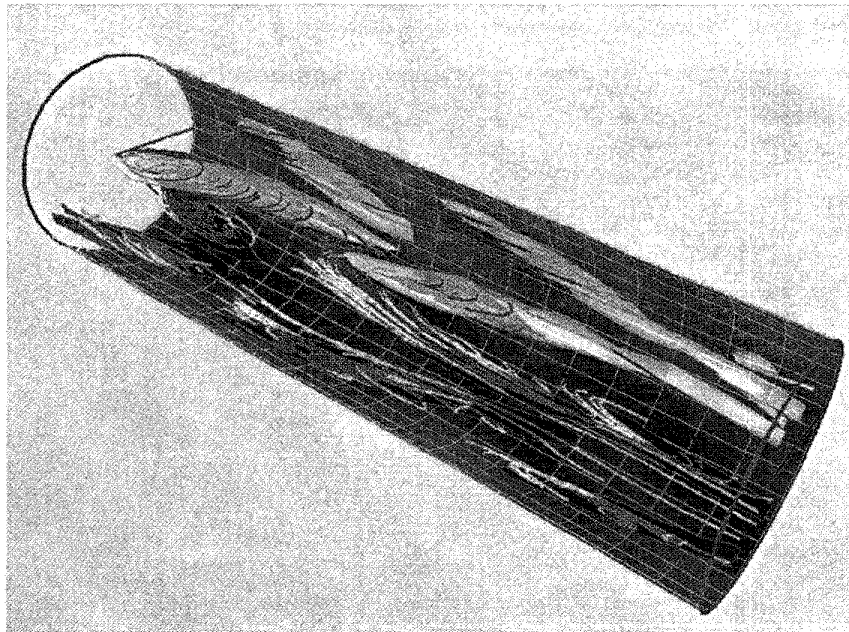


Figure 9: Transitional pipe flow with semi-transparent isosurfaces of $Q = 0.05$, and streamlines through grid nodes where $Q \geq 0.05$. The upper half of the pipe has yellow isosurfaces and light blue streamlines, the lower half has blue isosurfaces and white streamlines.

Selective Visualization of Vortices in Hydrodynamic Flows
 I. Ari Sadarjoen, Frits H. Post, Bing Ma, David C. Banks, Hans-Georg Pagendarm